Structural Engineering and Mechanics, *Vol. 58, No. 2 (2016) 243-257*
DOI: http://dx.doi.org/10.12989/sem.2016.58.2.243

Seismic resistance of dry stone arches under in-plane seismic loading

Ivan Balic*, Nikolina Zivaljic[a], Hrvoje Smoljanovic[b] and Boris Trogrlic[c]

Faculty of Civil Engineering, Architecture and Geodesy, University of Split, Matice hrvatske 15, 21000 Split, Croatia

(Received August 26, 2015, Revised December 27, 2015, Accepted January 11, 2016)

Abstract. The aim of this study is to investigate the seismic resistance of dry stone arches under in-plane seismic loading. For that purpose, several numerical analyses were performed using the combined finite-discrete element method (FDEM). Twelve types of arches with different ratios of a rise at the mid-span to the span, different thicknesses of stone blocks and different numbers of stone blocks in the arch were subjected to an incremental dynamic analysis based on excitation from three real horizontal and vertical ground motions. The minimum value of the failure peak ground acceleration that caused the collapse of the arch was adopted as a measure of the seismic resistance. In this study, the collapse mechanisms of each type of stone arch, as well as the influence of the geometry of stone blocks and stone arches on the seismic resistance of structures were observed. The conclusions obtained on the basis of the performed numerical analyses can be used as guidelines for the design of dry stone arches.

Keywords: seismic resistance; dry stone arch; seismic loading; stability; combined finite-discrete element method (FDEM)

1. Introduction

Arches are one of the most common structural shapes present in the worldwide architectural heritage. They have been used in architecture since the early beginnings of the building of settlements, religious structures, monuments, bridges and vaults. Dry stone arches are often used, probably due to their simple geometry, construction and their ability to transfer external load by a compressive stress (Boyd 1978, DeJong 2009). Some of these types of structures are situated in seismically active areas. Further, most of these structures are of historical and architectural value, therefore accurate and precise tools of analysis are needed to ensure reliable predictions of their seismic safety.

Arches are rarely found as detached structures. They are usually located within bridges and walls. If one takes into account the influence of surrounding walls or a bridge over arches, the number of variables that can affect the stability of such a structure increases. Therefore, to reduce

*Corresponding author, Ph.D., E-mail: ivan.balic@gradst.hr
[a]Assistant Professor
[b]Research Assistant

http://www.techno-press.org/?journal=sem&subpage=8 ISSN: 1225-4568 (Print), 1598-6217 (Online)

the number of parameters and reach some general conclusions, this article focuses on the seismic resistance of dry stone arches. Investigation into a wider influence of boundary conditions (such as walls or bridges over the arches) is indicated for further research.

To determine the collapse and seismic resistance of masonry structures, as well as arch bridges and masonry arches in general, one can use different numerical methods. The finite element method is the most commonly used method for the analysis of a structure. It has found its application in the analysis of block and block-like structures and stone masonry structures (Croci 1995, Lourenço and Rots 1997, Macchi 2001, Pelà *et al*. 2009, Erdolen and Doran 2012, Milani and Lourenço 2012, Turker 2014). In the framework of this method, the material of a structure is mostly regarded as a fictitious, homogeneous, orthotropic continuum where the average stress and strain relation is obtained either experimentally or by homogenization techniques. The disadvantages of modelling masonry structures as a continuum lie in the fact that such models are unable to take into account the appearance of large discontinuities in the displacement field between the blocks, as well as to simulate the mechanical interaction between blocks. This is important in the analysis of structures exposed to an intensive seismic load and in the analysis of a progressive collapse of masonry structures. Drosopoulos *et al*. (2008) investigated the influence of geometry and the movement of abutments on the collapse of stone arch bridges using the finite element method.

For the analysis of problems with a mechanical interaction between several blocks that can have finite rotations and displacements, numerical models based on the discrete element method were developed. The original discrete element method was initially oriented towards the study of jointed rock (Cundall 1971) and was later extended to other engineering applications including the modelling of masonry structures (Pagnoni 1994, Lemos 1998, Sincraian 2001, Bićanić *et al*. 2003, Rafiee *et al*. 2008, Rafiee and Vinches 2013). The general idea behind various applications of the discrete element method in masonry is an idealization of material as a discontinuum where joints are modelled as contact surfaces between different blocks. This approach is suitable for modelling different types of non-linear behaviour, including large displacements and rotation with complete detachment of blocks. A disadvantage of models based on the discrete element method is their inability to account for the state of stress and strain within the discrete element.

Bernat-Maso *et al*. (2012) used an experimental testing of masonry arches to validate different methods of analysis. DeJong *et al*. (2008) evaluated the susceptibility of masonry arches to earthquake loading through experimental testing.

Recently, an increasing number of models have attempted to combine the advantages of both finite and discrete element method (Petrinic 1996, Barbosa 1996, Mamaghani *et al*. 1999). Pérez-Aparicio *et al*. (2013) investigated the behaviour of masonry arches using a discontinuous deformation analysis. One of these methods is the combined finite-discrete element method (FDEM) developed by Munjiza (Munjiza 2004, Munjiza *et al*. 2012). The combined FDEM method, the subject of this paper, is based on a simulation of the behaviour of a large number of discrete elements which can be found in interaction. Within the framework of this method, discrete elements are discretized by constant-strain, triangular finite elements that enable deformability of discrete elements. Material non-linearity, including fracture and fragmentation of discrete elements, is considered through contact elements (Munjiza *et al*. 1999) that are implemented within a finite element mesh. The contact interaction between discrete elements, including friction, is taken into account by a distributed potential contact force (Munjiza 2004). The main processes included in the FDEM method are contact detection, contact interaction, finite strain elasticity, fracture and fragmentation, all of which are explained below. To take all these effects into account,

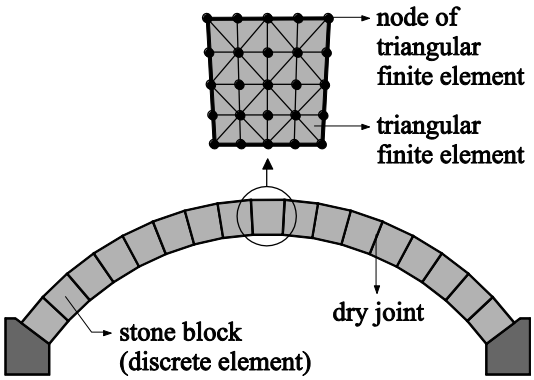

Fig. 1 Discretization of a dry stone masonry structure

appropriate algorithms were developed within the scope of this method (Munjiza 2004).

The FDEM method was successfully applied in the analysis of dry stone masonry structures and it showed good agreement with experimental results (Smoljanovic *et al*. 2013). This model is capable of predicting the collapse mechanism of dry stone masonry structures under seismic loads, as well as determining the safety of a structure by determining the value of the collapse load. To identify the influence of the geometry of a dry stone arch on seismic resistance, several numerical analyses using the combined finite-discrete element method were performed in this research. Twelve types of arches with different ratios of a rise at the mid-span to the span, different thicknesses of stone blocks and different numbers of stone blocks in the arch were subjected to an incremental dynamic analysis based on excitation from three real ground motions. The seismic resistance and collapse mechanisms for each type of arch were analysed on the basis of these results. Finally, based on the analyses performed in this study, recommendations for the design of stone arches with a greater seismic resistance were given.

2. The basics of the combined finite-discrete element formulation

2.1 Discretization of structure

Discretization of a dry stone masonry structure in the framework of the FDEM method is shown in Fig. 1. Each stone block is modeled as a discrete element, and each discrete element has its own finite element mesh which is used for the analysis of particle deformability. Masses are lumped into the nodes of finite elements, as shown in Fig. 1.

Given that the strength of stone is mostly much greater than the effective stress level occurring in stone structures (Oliveira 2003, Smoljanovic *et al*. 2013) and that, consequently, structural failure occurs mainly due to the loss of stability caused by relative displacements between blocks under the influence of a horizontal force, the cracking of stone blocks has not been considered in the performed analysis.

2.2 Deformability of finite elements

In the combined finite-discrete element method, the geometry of a three-noded, triangular finite

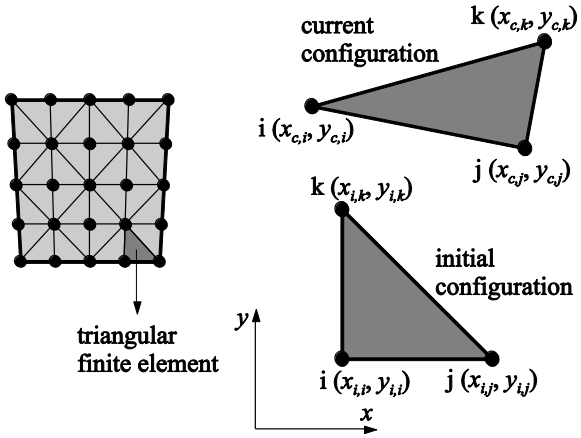

Fig. 2 Initial and current configuration of a triangular finite element

element is defined by global coordinates of each node (x, y), where (x_i, y_i) represent the coordinates of their initial configuration and (x_c, y_c) the coordinates of their current configuration (see Fig. 2). Since discrete elements change their positions in space, their displacements can be divided into two different components: displacements of discrete elements as solid bodies which cause translation and rotation and displacements causing deformations in shape and volume. Displacements of a deformable body involving rotation and deformation in the vicinity of a certain point are defined by the deformation gradient **F** (Munjiza 2004).

As a consequence of utilising triangular, three-noded finite elements, the deformation gradient is constant in all the points of the triangle and it can be obtained as follows

$$\mathbf{F} = \begin{bmatrix} x_{c,j} - x_{c,i} & x_{c,k} - x_{c,i} \\ y_{c,j} - y_{c,i} & y_{c,k} - y_{c,i} \end{bmatrix} \begin{bmatrix} x_{i,j} - x_{i,i} & x_{i,k} - x_{i,i} \\ y_{i,j} - y_{i,i} & y_{i,k} - y_{i,i} \end{bmatrix}^{-1} \tag{1}$$

Knowing the deformation gradient **F**, it is possible to calculate the Green-St. Venant strain tensor $\breve{\mathbf{E}}$ from the following expression

$$\breve{\mathbf{E}} = \frac{1}{2}\left(\mathbf{F}\,\mathbf{F}^T - \mathbf{I}\right) \tag{2}$$

Adopting the linear-elastic relationship between the stress and strain, the Cauchy stress tensor **T** can be obtained from the following expression

$$\mathbf{T} = \frac{E}{1+\upsilon}\breve{\mathbf{E}} + \frac{E}{1-2\upsilon}\varepsilon_v \mathbf{I} + \bar{\mu}\mathbf{D} \tag{3}$$

where E is the modulus of elasticity, υ is the Poisson ratio, ε_v is the volume deformation expressed by the following equation:

$$\varepsilon_v = \varepsilon_{xx} + \varepsilon_{yy} + \varepsilon_{zz} \tag{4}$$

where the last element on the right-hand side of Eq. (3) represents the contribution of the deformation velocity, where $\bar{\mu}$ is the damping coefficient and **D** is the rate of the deformation tensor (Munjiza *et al*. 1995).

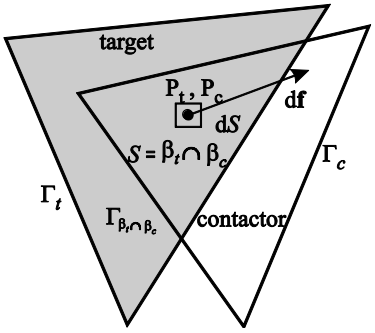

Fig. 3 Contact force due to an infinitesimal overlap around points P_t and P_c

The force belonging to each node and acting per unit of length on the side of a triangular finite element is obtained by directly integrating the strain tensor according to the following expression

$$\begin{bmatrix} f_x \\ f_y \end{bmatrix} = \frac{1}{2}\mathbf{T}\begin{bmatrix} n_{x,c} \\ n_{y,c} \end{bmatrix} \tag{5}$$

where $n_{x,c}$ and $n_{y,c}$ present components of the unit outer normal to the side of the triangular finite element.

2.3 Contact detection and interaction

The purpose of the contact detection algorithm is to detect pairs of discrete elements that are close to each other and eliminate those that are far apart and cannot establish contact. To this end, an NBS (no binary search) contact detection algorithm (Munjiza 2004, Munjiza *et al*. 1998) was implemented in the FDEM code.

Contact interaction and friction between discrete elements are taken into account via a distributed potential contact force (Munjiza 2004). In FDEM, a penalty function method based on potential contact force is employed to calculate the normal contact force. This method is based on the assumption that contact pairs (contactor and target) tend to collide and generate distributed contact forces.

The total contact force $\mathbf{f}_c$ is obtained by integrating the infinitesimal contact force d**f** (see Fig. 3), which leads to

$$\mathbf{f}_c = \int_{S=\beta_t \cap \beta_c} p\left(grad\varphi_c - grad\varphi_t\right)dS \tag{6}$$

where p is the penalty term, φ_c and φ_t are potential fields defined in contactor and target, respectively (Munjiza and Andrews 2000). The calculated contact force is distributed around the nodes surrounding the contact to preserve the system from artificial stress concentration. By replacing the integration over finite elements with the equivalent integration over finite element boundaries (Munjiza 2004), the following equation for contact force $\mathbf{f}_c$ is obtained

$$\mathbf{f}_c = \sum_{i=1}^{n}\sum_{j=1}^{n}\int_{\Gamma_{\beta_{c_i} \cap \beta_{t_j}}} \mathbf{n}_{\Gamma_{\beta_{c_i} \cap \beta_{t_j}}}\left(\varphi_{c_i} - \varphi_{t_j}\right)d\Gamma \tag{7}$$

where β_c and β_t are the contactor and target discrete elements, respectively; **n** is the outward unit

normal to the boundary of the overlapping area and φ is a potential function. The integration over finite element boundaries can be written as a summation of the integration over the edges of the finite elements.

The total contact force exerted by the target triangle on an element edge is given by the area of the diagram of the potential over the edge

$$\mathbf{f}_{c,edge} = \frac{1}{\mathbf{u}^2}\mathbf{u}\int_0^L p\varphi(v)dv \tag{8}$$

where the term $\mathbf{u}^2$ comes from the fact that vector $\mathbf{u}$, which is orthogonal to the edge of the finite element, and the tangential vector v are not unit vectors (Munjiza 2004). The calculated elemental contact force is distributed around the nodes surrounding the contact to preserve the system from artificial stress concentration. The well-known, classic, Coulomb-type friction is implemented and described as follows:

$$\mathbf{f}_t = -k_t\,\boldsymbol{\delta}_t \tag{9}$$

where $\mathbf{f}_t$ is the tangential elastic contact force, k_t is the penalty term for friction, and $\boldsymbol{\delta}_t$ is the tangential displacement vector between particles (Xiang *et al*. 2009).

If $\mathbf{f}_t$ is greater than the friction force satisfying the Coulomb-type friction law, $|\,\mathbf{f}_t\,| > \mu|\,\mathbf{f}_n\,|$, the particles slide over each other, and the tangential force is calculated using the total normal elastic contact force $\mathbf{f}_n$

$$\mathbf{f}_t = -\mu\,\mathbf{f}_n \tag{10}$$

where μ is the coefficient of sliding friction.

2.4 Time integration of equations of motion

In the combined finite-discrete element method, the mass of a system is concentrated in the nodes of finite elements (see Fig. 4), which leads to a lumped-mass model.

Time integration of the equations of motion in time was conducted explicitly for each corresponding node by means of the finite differences method (Munjiza 2004), which is conditionally stable and whose stability and accuracy depend on the choice of a time step. The description of the update of variables can be written as

$$\begin{aligned}\mathbf{v}_{i,t+\Delta t/2} &= \mathbf{v}_{i,t-\Delta t/2} + \Delta t\,\mathbf{f}_{i,t}\,/\,m_i \\ \mathbf{x}_{i,t+\Delta t} &= \mathbf{x}_{i,t} + \Delta t\,\mathbf{v}_{i,t+\Delta t/2}\end{aligned} \tag{11}$$

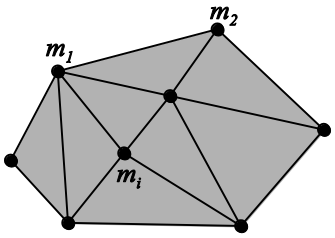

Fig. 4 Lumped-mass model

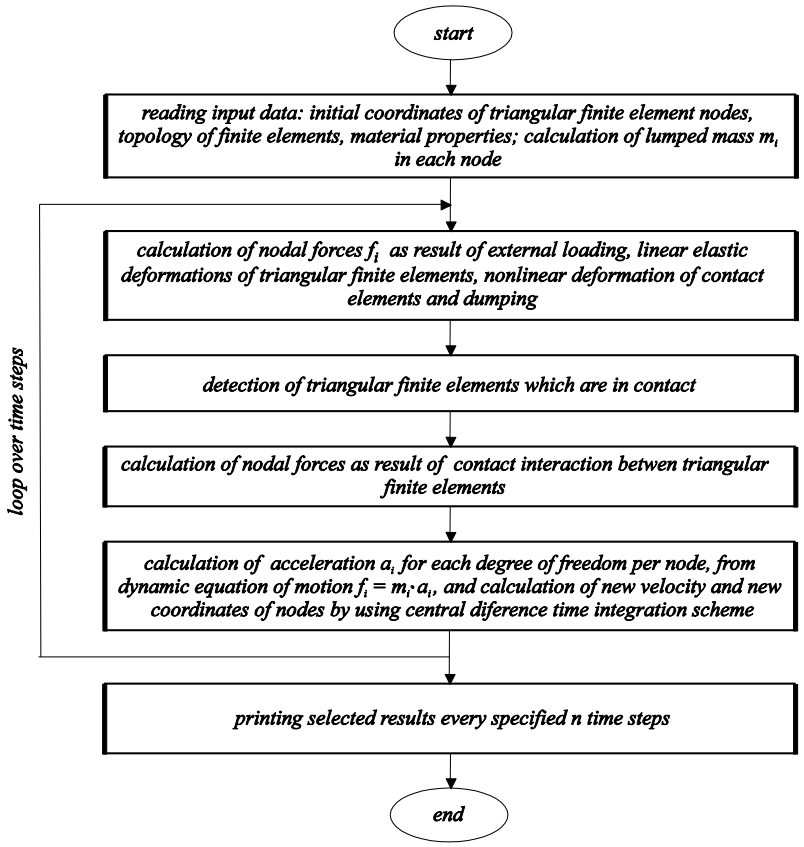

Fig. 5 Flowchart of the numerical procedure

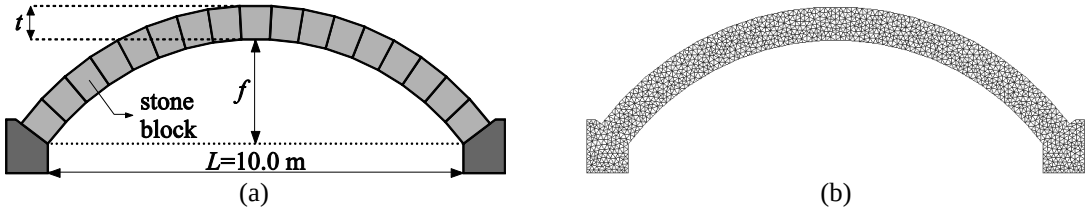

Fig. 6 Dry stone arch: (a) geometry (b) finite element mesh

where $\mathbf{x}_i$, $\mathbf{v}_i$, $\mathbf{f}_i$, m_i are the displacement vector, the velocity vector, the total force vector and the mass of each node, respectively, and Δt is a time step.

Fig. 5 shows a flowchart of the presented numerical procedure.

3. Numerical analyses and discussion

To identify the influence of the geometry of a dry stone arch on its seismic resistance, several numerical analyses were performed using the combined finite-discrete element method. Twelve types of arches (A1, A2, B1, B2, C1, C2, D1, D2, E1, E2, F1, F2) with different ratios of a rise at

the mid-span f to the span L, different thicknesses of stone blocks t and different numbers of stone blocks in the arch were subjected to an incremental dynamic analysis based on excitation from three real ground motions. The geometry of the dry stone arch with the symbols f, L and t is shown in Fig. 6(a), and a typical finite element mesh is shown in Fig. 6(b).

Material characteristics used in the numerical analyses, which proved suitable for analysis of dry stone masonry structures, were adopted according to bibliographic information found in Smoljanovic (2013) and shown in Table 1.

The geometry of dry stone arches with a rise at the mid-span of f=2.5 m are shown in Fig. 7.

The geometry of dry stone arches with a rise at the mid-span of f=4.0 m are shown in Fig. 8.

Table 1 Material characteristics of stone

Density ρ (kg/m^3)	Modulus of elasticity E (MPa)	Friction coefficient μ	Damping coefficient $\bar{\mu}$
2600	48400	0.6	$4.5 \cdot 10^6$

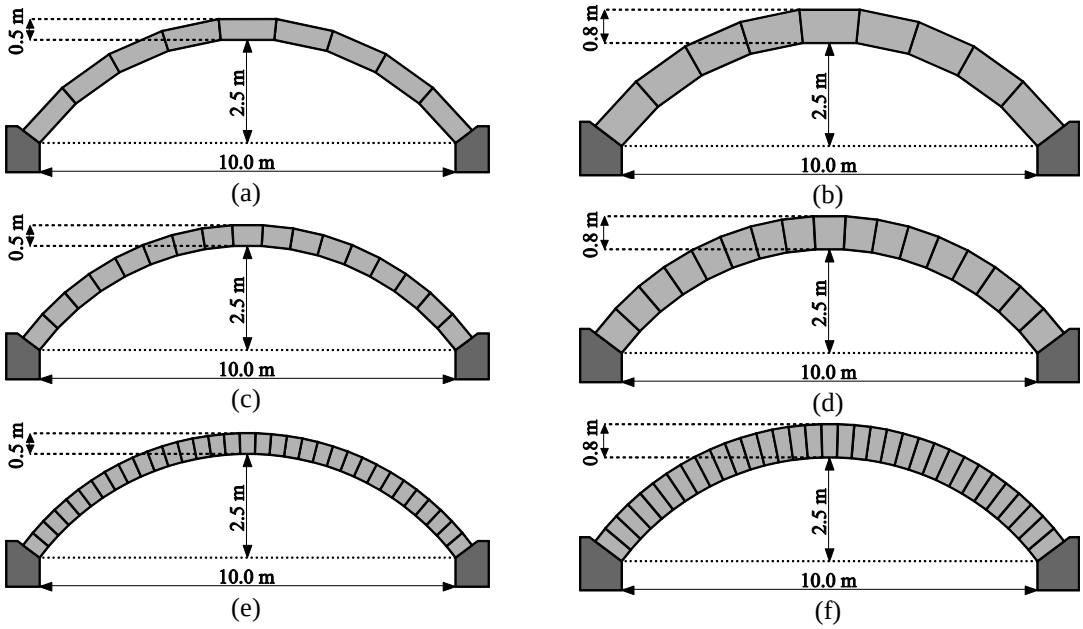

Fig. 7 Geometry of the arches type: (a) A1 (b) A2 (c) B1 (d) B2 (e) C1 (f) C2

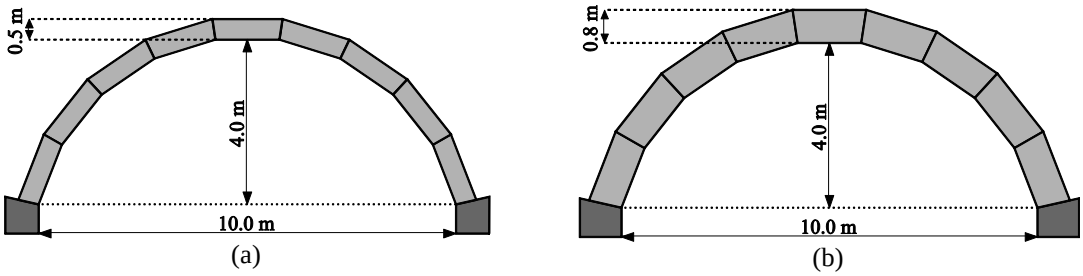

Fig. 8 Geometry of the arches type: (a) D1 (b) D2 (c) E1 (d) E2 (e) F1 (f) F2

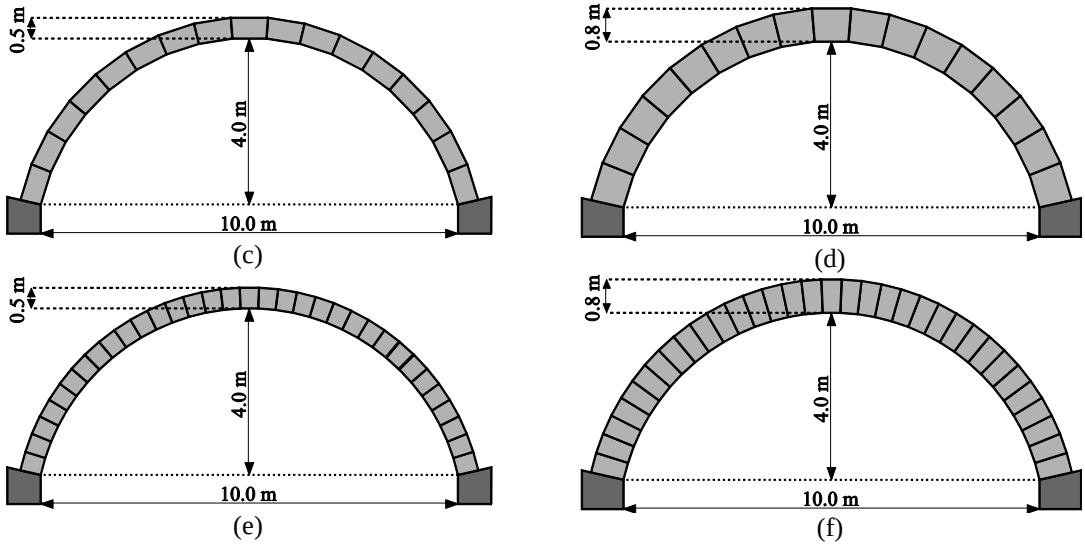

Fig. 8 Continued

In the presented numerical analyses, twelve different types of dry stone arches were exposed to horizontal and vertical ground acceleration whose values were taken from accelerograms of three real earthquakes recorded on the rock soil. The horizontal accelerograms were first scaled to the peak ground acceleration a_g of 0.30 g and the arches were exposed to that excitation with associated vertical amplitudes. After that, the horizontal and associated vertical accelerations were gradually increased until the collapse of the arch.

The earthquake accelerograms were taken from the European Strong-Motion Database (2014). The selected earthquakes are Campano Lucano (Italy)-1980, Valnerina (Italy)-1979 and Calabria (Italy)-1978.

Figs. 9, 10 and 11 show the dynamic behaviour of the type A1 dry stone arch exposed to the failure peak ground acceleration a_g equal to the seismic excitation generated by the Campano Lucano, Valnerina and Calabria earthquakes (a_g=1.00 g, a_g=2.00 g and a_g=2.20 g, respectively).

Fig. 9 Behaviour of the type A1 arch exposed to the failure peak ground acceleration of the Campano Lucano earthquake (a_g=1.00 g) in time periods of: (a) t=13.60 s (b) t=14.96 s (c) t=15.38 s

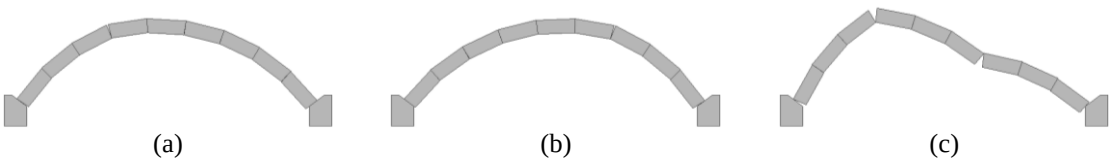

Fig. 10 Behaviour of the type A1 arch exposed to the failure peak ground acceleration of the Valnerina earthquake (a_g=2.00 g) in time periods of: (a) t=5.85 s (b) t=6.95 s (c) t=8.38 s

(a) (b) (c)

Fig. 11 Behaviour of the type A1 arch exposed to the failure peak ground acceleration of the Calabria earthquake (a_g=2.20 g) in time periods of: (a) t=4.77 s (b) t=10.23 s (c) t=12.80 s

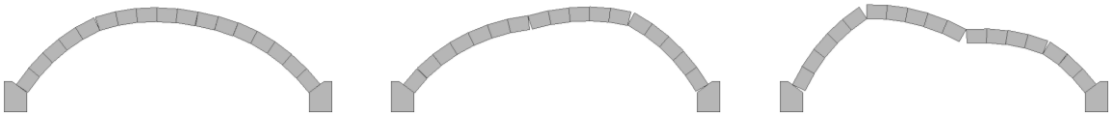

(a) (b) (c)

Fig. 12 Behaviour of the type B1 arch exposed to the failure peak ground acceleration of the Campano Lucano earthquake (a_g=1.20 g) in time periods of: (a) t=13.31 s (b) t=14.41 s (c) t=16.17 s

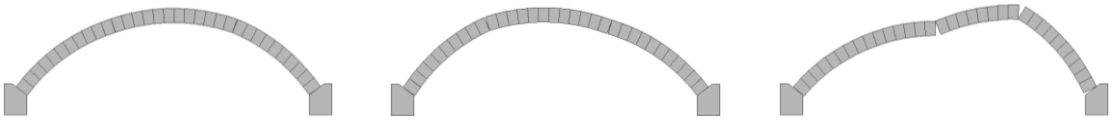

(a) (b) (c)

Fig. 13 Behaviour of the type C1 arch exposed to the failure peak ground acceleration of the Campano Lucano earthquake (a_g=1.40 g) in time periods of: (a) t=10.87 s (b) t=11.29 s (c) t=13.75 s

(a) (b) (c)

Fig. 14 Behaviour of the type A2 arch exposed to the failure peak ground acceleration of the Campano Lucano earthquake (a_g=2.00 g) in time periods of: (a) t=11.55 s (b) t=12.76 s (c) t=14.52 s

(a) (b) (c)

Fig. 15 Behaviour of the type B2 arch exposed to the failure peak ground acceleration of the Campano Lucano earthquake (a_g=2.10 g) in time periods of: (a) t=10.87 s (b) t=12.25 s (c) t=13.13 s

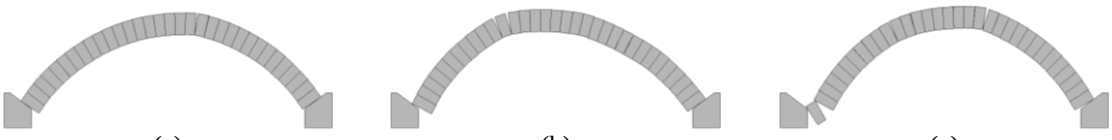

(a) (b) (c)

Fig. 16 Behaviour of the type C2 arch exposed to the failure peak ground acceleration of the Campano Lucano earthquake (a_g=2.20g) in time periods of: (a) t=10.98 s (b) t=12.34 s (c) t=12.61 s

The performed numerical analysis of the seismic resistance for all types of arches indicated that the Campano Lucano earthquake was the most unfavourable, as it is shown in Table 2. Therefore, the results of the numerical analysis are shown below only for the Campano Lucano earthquake.

Figs. 12-16 show the behaviour of dry stone arches with the ratio of the rise at the mid-span to the span f/L=0.25 exposed to failure peak ground acceleration.

Figs. 17-22 show the behaviour of dry stone arches with the ratio of the rise at the mid-span to the span f/L=0.40 exposed to failure peak ground acceleration.

As the result of the numerical analysis, the minimum values of the ratio a_g/g causing the loss of stability of each type of stone arch are presented in Table 2. The minimum value $(a_g/g)_{min}$ of the dynamic response for a series of three earthquake excitations was adopted as a measure of the seismic resistance.

(a) (b) (c)

Fig. 17 Behaviour of the type D1 arch exposed to the failure peak ground acceleration of theCampano Lucano earthquake (a_g=0.45 g) in time periods of: (a) t=12.83 s (b) t=13.42 s (c) t=14.15 s

(a) (b) (c)

Fig. 18 Behaviour of the type E1 arch exposed to the failure peak ground acceleration of the Campano Lucano earthquake (a_g=0.50 g) in time periods of: (a) t=12.85 s (b) t=13.79 s (c) t=14.15 s

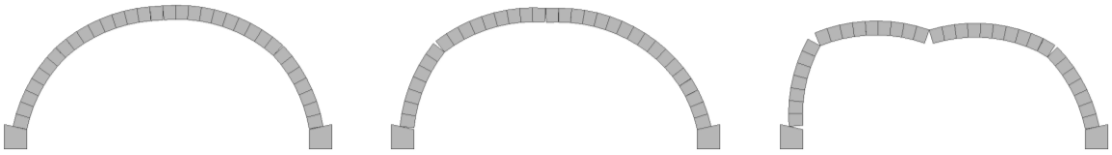

(a) (b) (c)

Fig. 19 Behaviour of the type F1 arch exposed to the failure peak ground acceleration of Campano Lucano earthquake (a_g=0.55 g) in time periods of: (a) t=12.96 s (b) t=13.66 s (c) t=14.12 s

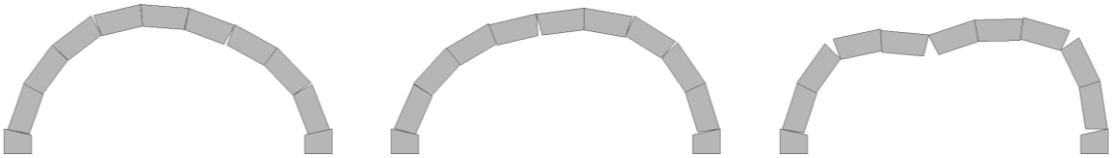

(a) (b) (c)

Fig. 20 Behaviour of the type D2 arch exposed to the failure peak ground acceleration of the Campano Lucano earthquake (a_g=1.35 g) in time periods of: (a) t=12.32 s (b) t=14.30 s (c) t=15.14 s

(a) (b) (c)

Fig. 21 Behaviour of the type E2 arch exposed to the failure peak ground acceleration of the Campano Lucano earthquake (a_g=1.40 g) in time periods of: (a) t=8.93 s (b) t=9.59 s (c) t=10.14 s

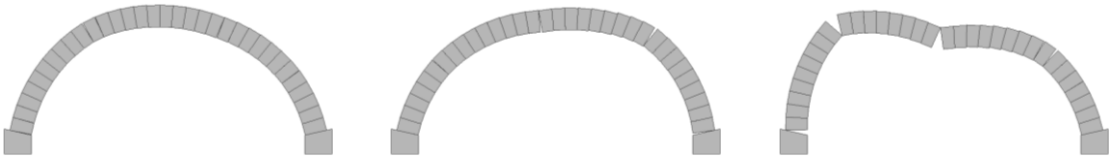

(a) (b) (c)

Fig. 22 Behaviour of the type F2 arch exposed to the failure peak ground acceleration of the Campano Lucano earthquake (a_g=1.40 g) in time periods of: (a) t=12.23 s (b) t=12.87 s (c) t=14.48 s

Table 2 The failure peak ground acceleration due to which the dry stone arches lose their stability

Arch type	a_g/g			$(a_g/g)_{min}$
	Campano Lucano	Valnerina	Calabria	
A1	1.00	2.00	2.20	1.00
B1	1.20	2.20	2.35	1.20
C1	1.40	2.10	2.55	1.40
A2	2.00	2.70	2.65	2.00
B2	2.10	2.75	2.75	2.10
C2	2.20	2.80	3.00	2.20
D1	0.45	0.85	1.15	0.45
E1	0.50	0.80	1.10	0.50
F1	0.55	0.90	1.10	0.55
D2	1.35	1.85	2.60	1.35
E2	1.40	1.90	2.20	1.40
F2	1.40	1.90	2.30	1.40

One of the most important parameters in the design and construction of arches is the ratio of the rise at the mid-span to the span of the arch *f/L*. The results of the numerical analyses presented in the Table 2 show that shallow dry stone arches (arches A1, A2, B1, B2, C1, C2) have greater seismic resistance in comparison to deep arches. This is due to the fact that arches with a higher ratio of the rise at the mid-span to the span *f/L* require less horizontal inertial force that causes separation of stone blocks and the occurrence of the mechanism.

Also, it can be observed that dry stone arches with a higher stone block thickness *t* (arches A2, B2, C2, D2, E2, F2) have greater seismic resistance in comparison to thinner arches. This is related to the thrust zone which, in blocks with higher thickness, is wide enough to transmit the whole thrust.

The presented results also indicate that arches with a larger number of stone blocks mostly possess higher seismic resistance in comparison to arches consisting of smaller number of stone blocks. The authors firmly believe that this is related to the fact that arches with larger number of stone blocks have greater possibility to change their shape in order to hold the thrust line inside the width of cross section.

From the obtained results, shown in Figs. 9 and 12-22, it can be observed that for the stone arches with a smaller ratio of the rise at the mid-span to the span *f/L*, especially for arches with higher thickness of stone blocks, the collapse occurs due to the sliding of the boundary blocks on the support. On the other hand, in the arches with a higher ratio of the rise at the mid-span to the span *f/L*, the collapse occurs as the appearance of the mechanism, i.e., formation of the minimum of four hinges. This is related to the fact that by increasing thickness of stone blocks, horizontal inertial force which causes separation of stone blocks increases, too, and in the case of shallow stone arches it can become bigger than frictional resistance between a stone block and the base. Also, it can be observed that for the dry stone arches with a higher ratio of the rise at the mid-span to the span *f/L*, regardless of the thicknesses and number of blocks, the collapse of arches occurs as the appearance of the mechanism, i.e., formation of the minimum of four hinges.

4. Conclusions

This paper presents the application of the combined FDEM method with the scope of identifying the influence of the geometry of dry stone arches on their seismic resistance. Twelve types of arches with different ratios of the rise at the mid-span to the span, different thicknesses of stone blocks and different numbers of stone blocks in the arch were subjected to an incremental dynamic analysis based on excitation from three ground motions. The minimum value of the failure peak ground acceleration that caused collapse of arches was adopted as a measure of the seismic resistance. Collapse mechanisms for each type of stone arch and their seismic resistance were observed.

Based on the numerical analyses performed in this paper, the following conclusions can be reached:

- Shallow dry stone arches have greater seismic resistance in comparison to deep arches.
- Dry stone arches with a higher stone block thickness have greater seismic resistance in comparison to thinner arches.
- Arches with a larger number of stone blocks mostly possess higher seismic resistance in comparison to arches consisting of smaller number of stone blocks.
- For the dry stone arches with a smaller ratio of the rise at the mid-span to the span, especially arches with higher thickness of stone blocks, the collapse occurs due to sliding of boundary blocks on the support, whereas in the arches with a higher ratio of the rise at the mid-span to the span, the collapse occurs as the appearance of the mechanism, i.e., formation of the minimum of four hinges.

References

Barbosa, B.E. (1996), “Discontinuous structural analysis”, *Proceedings of the 11th World Conference on Earthquake Engineering*, Elsevier, Paper No. 830.

Bernat-Maso, E., Gil, L. and Marce-Nogue, J. (2012), "The structural performance of arches made of few vossoirs with dry-joints", *Struct. Eng. Mech.*, **44**(6), 775-799.
Bićanić, N., Stirling, C. and Pearce, C.J. (2003), "Discontinuous modelling of masonry bridges", *Comput. Mech.*, **31**(1-2), 60-68.
Boyd, T.D. (1978), "The arch and the vault in Greek architecture", *Am. J. Archaeol.*, **82**(1), 83-100.
Croci, G. (1995), "The Colosseum: safety evaluation and preliminary criteria of intervention", *International Seminar on Structural Analysis of Historical Constructions-SAHC*, Barcelona, Spain, 154-165.
Cundall, P.A. (1971), "A computer model for simulating progressive large scale movements in blocky rock systems", *Proceedings of the Symposium of International Society for Rock Mechanics*, International Society for Rock Mechanics (ISRM), Nancy, France, Vol. 1, Paper No. II-8, 132-150.
DeJong, M.J. (2009), "Seismic assessment strategies for masonry structures", Ph.D. Dissertation, Massachusetts Institute of Technology, Massachusetts, USA.
DeJong, M.J., De Lorenzis, L., Adams, S. and Ochsendorf, J.A. (2008), "Rocking stability of masonry arches in seismic regions", *Earthq. Spectra*, **24**(4), 847-865.
Drosopoulos, G.A., Stavroulakis, G.E. and Massalas, C.V. (2008), "Influence of the geometry and the abutments movement on the collapse of stone arch bridges", *Constr. Build. Mater.*, **22**, 200-210.
Erdolen, A. and Doran, B. (2012), "Interval finite element analysis of masonry-infilled walls", *Struct. Eng. Mech.*, **44**(1), 73-84.
European Strong-Motion Database (2014), http://www.isesd.hi.is/ESD_Local/frameset.htm.
Lemos, J.V. (1998), "Discrete element modelling of the seismic behaviour of stone masonry arches", *Proceedings of the 4th International Symposium on Computer Methods in Structural Masonry*, E & FN Spon, London, 220-227.
Lourenço, P.B. and Rots, J.G. (1997), "Multisurface interface model for analysis of masonry structures", *J. Eng. Mech.*, **123**(7), 660-668.
Macchi, G. (2001), "Diagnosis of the facade of St. Peter's Basilica in Rome", Historical Constructions, University of Minho, Guimarães, 309-317.
Mamaghani, I.H.P., Aydan, O. and Kajikawa, Y. (1999), "Analysis of masonry structures under static and dynamic loading by discrete finite element method", *Journal of Structural Mechanics and Earthquake Engineering*, Japan Society of Civil Engineers (JSCE), No. 626/I-48, 1-12.
Milani, G. and Lourenço, P.B. (2012), "3D non-linear behavior of masonry arch bridges", *Comput. Struct.*, **110-111**, 133-150.
Munjiza, A. (2004), *The Combined Finite-Discrete Element Method*, John Wiley & Sons, London, UK.
Munjiza, A. and Andrews, K.R.F. (2000), "Penalty function method for combined finite-discrete element system comprising large number of separate bodies", *Int. J. Numer. Meth. Eng.*, **49**(11), 1377-1396.
Munjiza, A., Andrews, K.R.F. and White, J.K. (1998), "NBS contact detection algorithm for bodies of similar size", *Int. J. Numer. Meth. Eng.*, **43**(1), 131-149.
Munjiza, A., Andrews, K.R.F. and White, J.K. (1999), "Combined single and smeared crack model in combined finite-discrete element method", *Int. J. Numer. Meth. Eng.*, **44**(1), 41-57.
Munjiza, A., Knight, E.E. and Rouiger, E. (2012), *Computational Mechanics of Discontinua*, John Wiley & Sons, London, UK.
Munjiza, A., Owen, D.R.J. and Bićanić, N. (1995), "A combined finite-discrete element method in transient dynamics of fracturing solids", *Eng. Comput.*, **12**(2), 145-174.
Oliveira, D.V. (2003), "Experimental and numerical analyses of blocky masonry structures under cyclic loading", Ph.D. Dissertation, University of Minho, Guimarães, Portugal.
Pagnoni, T. (1994), "Seismic analysis of masonry and block structures with the discrete element method", *Proceedings of the 10th European Conference on Earthquake Engineering*, A.A. Balkema, Rotterdam, Vol. 3, 1669-1674.
Pelà, L., Aprile, A. and Benedetti, A. (2009), "Seismic assessment of masonry arch bridges", *Eng. Struct.*, **31**(8), 1777-1788.
Pérez-Aparicio, J.L., Bravo, R. and Ortiz, P. (2013), "Refined element discontinuous numerical analysis of dry-contact masonry arches", *Eng. Struct.*, **48**, 578-587.

Petrinic, N. (1996), "Aspects of discrete element modelling involving facet-to-facet contact detection and interaction", Ph.D. Dissertation, University of Wales, UK.

Rafiee, A. and Vinches, M. (2013), "Mechanical behaviour of a stone masonry bridge assessed using an implicit discrete element method", *Eng. Struct.*, **48**, 739-749.

Rafiee, A., Vinches, M. and Bohatier, C. (2008), "Application of the NSCD method to analyse the dynamic behaviour of stone arched structures", *Int. J. Solid. Struct.*, **45**(25-26), 6269-6283.

Sincraian, G.E. (2001), "Seismic behaviour of blocky masonry structures. A discrete element method approach", Ph.D. Dissertation, Instituto Superior Tecnico, Lisbon, Portugal.

Smoljanovic, H. (2013), "Seismic analysis of masonry structures with finite-discrete element method", Ph.D. Dissertation, University of Split, Croatia.

Smoljanovic, H., Zivaljic, N. and Nikolic, Z. (2013), "A combined finite-discrete element analysis of dry stone masonry structures", *Eng. Struct.*, **52**, 89-100.

Turker, T. (2014), "Structural evaluation of Aspendos (Belkis) Masonry Bridge", *Struct. Eng. Mech.*, **50**(4), 419-439.

Xiang, J., Munjiza, A., Latham, J.P. and Guises, R. (2009), "On the validation of DEM and FEM/DEM models in 2D and 3D", *Eng. Comput.*, **26**(6), 673-687.

CC